Progress In Electromagnetics Research, Vol. 109, 63–81, 2010

SPARSE RECONSTRUCTION FOR SAR IMAGING BASED ON COMPRESSED SENSING

S.-J. Wei, X.-L. Zhang, J. Shi, and G. Xiang

School of Electronic Engineering
University of Electronic Science and Technology of China
Chengdu 610054, China

Abstract—Synthetic Aperture Radar (SAR) can obtain a two-dimensional image of the observed scene. However, the resolution of conventional SAR imaging algorithm based on Matched Filter (MF) theory is limited by the transmitted signal bandwidth and the antenna length. Compressed sensing (CS) is a new approach of sparse signals recovered beyond the Nyquist sampling constraints. In this paper, a high resolution imaging method is presented for SAR sparse targets reconstruction based on CS theory. It shows that the image of sparse targets can be reconstructed by solving a convex optimization problem based on L1 norm minimization with only a small number of SAR echo samples. This indicates the sample size of SAR echo can be considerably reduced by CS method. Super-resolution property and point-localization ability are demonstrated using simulated data. Numerical results show the presented CS method outperforms the conventional SAR algorithm based on MF even though small sample size of SAR echo is used in this method.

1. INTRODUCTION

Synthetic aperture radar (SAR) can obtain high resolution images of illuminated scene under all weather circumstances. It is an important imaging and detecting tool for many remote sensing applications in military and civilian fields, including topographic mapping, target identification, classification, and flight navigation etc. For conventional standard SAR imaging, the high resolution of range direction is obtained by the pulse compression of chirp signal,

Received 8 August 2010, Accepted 30 September 2010, Scheduled 13 October 2010
Corresponding author: Shun-Jun Wei (grinwshj@163.com).

and the high resolution of azimuth direction is received through the synthetic aperture formed by platform movement [1]. Therefore, the echo samples of standard SAR follow Shannon's celebrated theorem: the sampling rate must be at least twice the maximum frequency of the echo signal (the so-call Nyquist rate) [2]. Till now, the most popular methods for SAR imaging are based on matched filtering (MF) theory [3], such as Range-Doppler algorithm [4], Chirp-Scaling algorithm [5], Spectral Analysis algorithm [6], etc. These algorithms are mostly based on the Fourier transform or time-frequency interpolation. The reflections are focused by coherent accumulation to generate an image of illuminated scene. However, these traditional SAR imaging methods based on MF have many obvious disadvantages: 1) the range resolution is limited by the bandwidth of transmitted signal, and the azimuth resolution is proportional to the antenna length which is limited by radar system, therefore high resolution SAR imaging is difficult to be achieved with low bandwidth and short aperture; 2) According to Nyquist rate, a large amount of echo samples must be collected which will lead to an excessive burden of acquired of SAR system; 3) the imaging results show serious sidelobe interference problems.

In recent years, a new approach named compressed sensing (CS) which applies to signal reconstruction has attracted more and more attention [7, 8]. CS indicates that certain signals and images can be recovered with far fewer samples or measurements than traditional method. The pre-condition of exact recovery by CS is that the signal is sparse or compressible in some domain such as time, space and frequency. Inspired by the idea of CS, more and more efficient schemes have been proposed for signal reconstruction at much smaller sampling rate than traditional Nyquist sampling theorem. Due to its compressed sampling and exact reconstruction ability, CS has been widely used in many applications, such as data acquisition, communications, remote sensing, computational biology, medicine imaging, radar, etc. [9–11]. Some applications in radar field are as following. A compressive sensing data acquisition and imaging system for Ground Penetrating Radar (GPR) was proposed in [12, 13]. Instead of sampling radar echo at Nyquist rate, linear projections for echo signal on some random vectors were used as measurements. A similar theme was presented for through-wall radar imaging [14]. In order to reduce the amount of stored SAR raw data, a method based on CS theory was proposed in [15]. A compressive radar imaging scheme based on CS was proposed in [16], the system can eliminate the need for the matched filter in the radar receiver and reduce the required receiver analog-to-digital conversion bandwidth. In [17], high resolution radar was proposed

by transmitting specially designed waveforms, where the theory of CS with random convolution was used by transmitting random noise-like signals. In [18], resolution enhancement for ISAR imaging under low SNR via CS was presented. We can see that CS has been got more and more attention in radar applications, such as to lighten up sampling burden and improve the resolution of radar system in recent years.

In some special applications (such as ships detecting and city area imaging), the main scattering targets distribute in a sparse way over illuminated scene. The number of dominant scatterers is much smaller than the number of overall samples. In such a case, SAR echo can be regarded as sparse signal. Thereby, a sparse reconstruction based on CS can be used in these applications. To overcome the resolution limitation of conventional SAR imaging method based on MF, we present a novel high resolution imaging method of SAR based on CS in this paper. The remarkable advantage of the presented CS method is that it can obtain higher resolution with fewer measured data than that obtained under the Nyquist rate. We apply CS to extract the main strong scattering coefficients by constructing a time-frequency overwhelming dictionary. Some numerical simulations are presented to evaluate the potential and limits for the presented method. The results show that the presented CS method outperforms the conventional imaging algorithm based on MF method.

This paper is organized into six sections as following. Section 2 gives a brief description of the basis theory of CS. Section 3 contains an introduction of standard SAR model and MF-based imaging method. Section 4 describes linear measurement model of SAR echo signal and presents the imaging algorithm based on CS. Numerical simulated results and algorithm performance are discussed in Section 5. Finally, a summary is given in Section 6.

2. BASIS THEORY OF CS

Compressed sensing (CS) is a new theory which enables the reconstruction of sparse signal using far fewer samples or measurements than Nyquist rate. Considering a discrete signal vector $x \in \mathbf{R}^N$, we say that it is K-sparse if at most $K \ll N$ of its coefficients is nonzero in an orthonormal basis or over-complete dictionary $\mathbf{\Psi} \in \mathbf{C}^{N \times N}$. Hence, the true information is contained in x which lives in at most K dimensions rather than N. The sparse signal can be expressed as

$$x = \mathbf{\Psi}\boldsymbol{\alpha} \tag{1}$$

where vector $\boldsymbol{\alpha} \in \mathbf{R}^N$ is the weighting coefficient. As the signal x has a sparse representation in $\mathbf{\Psi}$, x can be well approximated by the best K term expression.

According to CS theory, the measured signal is acquired by linear projections $y = \mathbf{\Phi}x$. It makes sense that only M samples of signal x need to be measured instead of N. Then, considering a linear measurements matrix $\mathbf{\Phi} \in \mathbf{C}^{M\times N}$ with $M < N$, the measurements signal $y \in \mathbf{R}^M$ is descried as

$$y = \mathbf{\Phi}x = \mathbf{\Phi\Psi}\boldsymbol{\alpha} = \mathbf{\Theta}\boldsymbol{\alpha} \tag{2}$$

where $\mathbf{\Theta} = \mathbf{\Phi\Psi}$ is a $M \times N$ matrix. This set of equations is underdetermined and (2) has infinitely many solutions. However, it is indeed possible to recover the sparse signal via CS when the matrix $\mathbf{\Phi}$ has the Restricted Isometry Property (RIP) of order K [9]. The RIP requires that

$$(1-\delta_K)\left\|\boldsymbol{\alpha}\right\|_2^2 \le \left\|\mathbf{\Theta}\boldsymbol{\alpha}\right\|_2^2 \le (1+\delta_K)\left\|\boldsymbol{\alpha}\right\|_2^2 \tag{3}$$

where $\boldsymbol{\alpha}$ is any vector having K nonzero coefficients, and $\delta_K \in (0,1)$. The smaller the value δ_K is, the better the sparse signal can be reconstructed. The RIP is closely related to an incoherency property. It is proved that random matrix performs well. If the number of measurements $M \ge O\left(K\log\left(N/K\right)\right)$, the K-sparse signal x can be exactly reconstructed with high probability [8].

Known the observed vector y and the measured matrix $\mathbf{\Theta}$, the signal x can be recovered from the solution of a convex optimization problem based on l_1 norm.

$$\min \left\|\boldsymbol{\alpha}\right\|_1 \ \text{s.t}\ y = \mathbf{\Theta}\boldsymbol{\alpha} \tag{4}$$

If noise is taken into account, the modified convex problem can be described as

$$\min \lambda\left\|\boldsymbol{\alpha}\right\|_1 \ \text{s.t}\ \ \left\|y - \mathbf{\Theta}\boldsymbol{\alpha}\right\|_2 < \varepsilon \tag{5}$$

where λ is weighted coefficient and ε bounds the amount of noise in measured data. Recently there are several sparse approximation algorithms to recover the sparse signal $\boldsymbol{\alpha}$ from measurements y. Such algorithms include basis pursuit (BP) [19], orthogonal match-pursuit (OMP) [20] and regularized orthogonal matching pursuit (ROMP) [21].

3. SAR MODEL AND IMAGING

Suppose SAR platform works in stripmap mode, X denotes azimuth direction and Z is altitude direction. The SAR platform flights along a track parallel to X axis at altitude H with the constant velocity v. θ denotes the incidence angle of radar. N_r and N_a denote sample size of range and azimuth respectively.

Suppose the antenna transmits a linear frequency modulated (LFM) signal as

$$s(t) = rect\left(\frac{t}{T}\right) \cdot \exp\left(j2\pi f_c t + j\pi f_{dr} t^2\right) \tag{6}$$

where f_c denotes carrier frequency, f_{dr} is LFM chirp rata, t is the fast-time, T is pulse repetition time, and $rect\,(t)$ denotes the unit rectangular function $rect\,(t) = 1$ when $|t| \in T/2$.

A referenced scatterer with the radar cross section (RCS) $\sigma(\mathbf{P}_w)$ is supposed at position $\mathbf{P}_w = (x, y, z)$. At slow-time n, the slant range from the scatterer $\mathbf{P}_w$ to the SAR platform is written as

$$R(n; \mathbf{P}_w) = \|\mathbf{P}(n) - \mathbf{P}_w\|_2 \approx R_{P_w} + (vn - x)^2 / (2R_{P_w}) \tag{7}$$

where $R_{P_w} = \sqrt{y^2 + H^2}$, $\mathbf{P}(n) = \mathbf{P}(0) + vn \cdot e$ denotes the position of SAR platform at slow-time, e is unit voter of azimuth direction. Then the echo signal of a referenced scatterer $\mathbf{P}_w$ can be expressed as (ignoring the antenna pattern)

$$s_m(t, n; \mathbf{P}_w) = \sigma(\mathbf{P}_w) \exp\left[j2\pi f_c(t-\tau) - j\pi f_{dr}(t-\tau)^2\right], \ |t| \in T/2 \tag{8}$$

where $\tau = 2R(n; \mathbf{P}_w)/C$ denotes the echo delay of the target, C is the speed of light in air. The de-chirping signal is the complex conjugate of the transmitted signal $s_f = s^*(t)$, the demodulated signal is described as

$$s_m(t, n; \mathbf{P}_w) = \sigma(\mathbf{P}_w) \exp(-j2\pi f_c \tau) \exp\left[j\pi f_{dr}(t-\tau)^2\right], \ |t| \in T/2 \tag{9}$$

For a measurement scene Ω, the echo signal can be written as

$$S_c(t, n) = \int\limits_{P_w \in \Omega} s_m(t, n; \mathbf{P}_w) d\mathbf{P}_w \tag{10}$$

For conventional matched filter (MF) method, for example, Range-Doppler (RD) algorithm, the image of illuminated scene is obtained by convoluting the received signal with its complex conjugated time reversed function. After 2-D focused by RD algorithm, the focused signal of SAR can be expressed as

$$S_o(t, n) \approx \int\limits_{P_w \in \Omega} \sigma(\mathbf{P}_w) \exp(-j\phi) \sin c\left[B_r(t-\tau)\right] \sin c\left[B_a\left(n - \frac{x}{v}\right)\right] d\mathbf{P}_w \tag{11}$$

where B_r denotes the bandwidth of LFM signal, B_a is the Doppler bandwidth of azimuth signal, and $\phi = 4\pi R/\lambda$ denotes the phase of target. According to (11), the resolution of range and azimuth directions can be calculate respectively as bellow.

$$\rho_r = \frac{C}{2B_r}, \quad \rho_a = \frac{D}{2} \tag{12}$$

where D denotes the antenna aperture in azimuth and λ denotes the radar wavelength. Hence, high range resolution is achieved by transmitting a wideband signal, and high azimuth resolution depends on the antenna aperture.

The Range-Doppler (RD) algorithm is the most commonly used algorithm for processing continuously collected SAR data into an image. In (12), the disadvantage of RD algorithm with chirp signal is that the imaging resolution is limited by bandwidth of signal. In addition, the existence of sidelobe prevents the discrimination of targets which are close to each other.

4. SAR IMAGING USING CS

An important prerequisite of CS sparse reconstruction is the signal must be sparse or compressible in certain representations. For SAR imaging, the true 3-D illuminated scene is projected into the 2-D range-azimuth plane, and then the projected targets are not always sparse. However, the target space can be regarded as sparse in some special applications in which only a small number of strong scatterers distribute in the illuminated scene, and the relatively few large coefficients of the scatterers can capture most of the information of scene, such as ocean ships monitoring, aircraft and spacecraft detecting, space debris imaging, and so on. Based on the feature of sparse signal in these applications, the image can be reconstructed by the signal of strong scattering centers using the theory of CS, and the weak scattering centers can be regarded as noise in image.

4.1. Create a Linear Model for SAR Echo Signal

Supposed $\mathbf{E} \in \mathbf{C}^{N_a \times N_r}$ denotes the scattering coefficients matrix of the 2-D illuminated scene. To easily facilitate the numerical implement, a long vector $\boldsymbol{\sigma} \in \mathbf{C}^{N \times 1}$ $(N = N_a \times N_r)$ is reformed by the columns of matrix $\mathbf{E}$. For the sparse targets scene, we assume that $\boldsymbol{\sigma}$ is K-sparse when only K $(K \ll N)$ of its coefficients is nonzero or greater than zero. The scattering coefficients $\boldsymbol{\sigma}$ can be expressed in a space orthogonal basis $\boldsymbol{\psi} \in \mathbf{R}^{N \times N}$ as

$$\boldsymbol{\sigma} = \boldsymbol{\psi}\boldsymbol{\alpha} \tag{13}$$

where $\boldsymbol{\alpha}$ is defined as the vector whose nonzero components are corresponding to the complex amplitudes of K strongest scattering centers.

In order to use CS, a linear measurement model of SAR should be created firstly. According to (5) and (6), in discrete scenarios the raw

echo signal of SAR can be expressed as

$$\begin{aligned} S_c(t,n) &= \sum_{i=1}^{N} \sigma_i \exp\left[j\pi f_{dr} \left(t - 2\frac{R(n;\mathbf{P}_i)}{C} \right)^2 - j4\pi f_c \frac{R(n;\mathbf{P}_i)}{C} \right] \\ &\quad \sum_{i=1}^{N} \sigma_i \exp\left[j\pi f_{dr} \left(t - 2\frac{R_{\mathbf{P}_w} + \frac{(vn-x)^2}{2R_{P_w}}}{C} \right)^2 - j4\pi f_c \frac{R_{\mathbf{P}_w} + \frac{(vn-x)^2}{2R_{P_w}}}{C} \right] \\ &= \sum_{i=1}^{N} \sigma_i \exp\left[-j\phi_i(t,n) \right] \end{aligned} \tag{14}$$

So, (14) can be expressed in vector form as

$$\begin{aligned} S_c &= \mathbf{A}_i^T \boldsymbol{\sigma} = \mathbf{A}_i^T \boldsymbol{\psi} \boldsymbol{\alpha} \\ \mathbf{A}_i &= \left\{ \exp\left[-j\phi_1(t,n) \right], \exp\left[-j\phi_2(t,n) \right], \ldots, \exp\left[-j\phi_N(t,n) \right] \right\}^T \end{aligned} \tag{15}$$

where $\mathbf{A}_i$ is interpreted as $N \times 1$ measurement vector at the slow-time n and fast-time t. Reformed by the columns, the vector of SAR echo signal can be written as

$$\mathbf{S} = \left[S_c(1,1), S_c(1,2), \ldots S_c(1,N_r), S_c(2,1), \ldots, S_c(N_a,N_r) \right]^T \tag{16}$$

The relation between the scattering coefficient vector $\boldsymbol{\sigma}$ and measured echo signal S can be written as linear representation model.

$$\mathbf{S} = \mathbf{A}\boldsymbol{\sigma} + n = \mathbf{A}\boldsymbol{\psi}\boldsymbol{\alpha} + n \tag{17}$$

$$\begin{aligned} \mathbf{A} &= \left[\mathbf{A}_1, \mathbf{A}_2, \ldots, \mathbf{A}_i, \ldots, \mathbf{A}_N \right]^T \\ &= \begin{bmatrix} e^{-j\phi_1(1,1)} & e^{-j\phi_2(1,1)} & \cdots & e^{-j\phi_N(1,1)} \\ e^{-j\phi_1(1,2)} & e^{-j\phi_2(1,2)} & \cdots & e^{-j\phi_N(1,2)} \\ \vdots & \vdots & \cdots & \vdots \\ e^{-j\phi_1(1,N_r)} & e^{-j\phi_2(1,N_r)} & \cdots & e^{-j\phi_N(1,N_r)} \\ e^{-j\phi_1(2,1)} & e^{-j\phi_2(2,1)} & \cdots & e^{-j\phi_N(2,1)} \\ \vdots & \vdots & \vdots & \vdots \\ e^{-j\phi_1(N_a,N_r)} & e^{-j\phi_2(N_a,N_r)} & \cdots & e^{-j\phi_N(N_a,N_r)} \end{bmatrix} \end{aligned} \tag{18}$$

where $\mathbf{A} \in \mathbf{C}^{N \times N}$ denotes the measurement matrix of SAR echo signal, and n represents the additive noise. The sampling rate of measured signal $\mathbf{S}$ obeys Nyquist theorem. However, according to CS theory, it is possible to recover the sparse signal with only a small number of samples of measured signal $\mathbf{S}$.

4.2. Random Range-azimuth Samples

In the spirit of CS, a very small number of "random" measurements carry enough information which can accomplish completely reconstruction for the signal. According to the feature of RIP in (3), all submatrices of $\mathbf{\Theta}$ are composed of K significant columns which should be nearly orthogonal. There are some well-known pairs of incoherent basis, such as randomly selected Fourier samples and random Gaussian matrix. Hence, we randomly select M $(O(K\log(N/K)) \leq M < N)$ rows of matrix $\mathbf{A}$ as the final measurement matrix $\mathbf{\Theta} \in \mathbf{R}^{M\times N}$ [8], and then the new measured signal can be expressed as

$$\mathbf{S}_p = \mathbf{\Phi}\mathbf{A}\boldsymbol{\psi}\boldsymbol{\alpha}+\mathbf{n} = \mathbf{\Theta}\boldsymbol{\alpha}+\mathbf{n} \tag{19}$$

where $\mathbf{\Phi}$ denotes a $M \times N$ matrix constructed by randomly selected M rows of $N \times N$ identity matrix which is taken as orthogonal basis. The randomly selected matrix can be written as

$$\mathbf{\Phi} = \begin{bmatrix} 1 & 0 & 0 & \dots & 0 & 0 \\ 0 & 0 & 1 & \dots & 0 & 0 \\ \vdots & \vdots & \vdots & \ddots & \vdots & \vdots \\ 0 & 0 & 0 & \dots & 0 & 1 \end{bmatrix}_{M\times N} \tag{20}$$

Essentially, the final measurement matrix $\mathbf{\Theta}$ is constructed by the measurement matrix $\mathbf{A}$ right multiplying with a random line selected matrix $\mathbf{\Phi}$. To facilitate, the random selection can be substituted for equal interval selection in practice.

Figure 1 shows acquisition of SAR echo data for traditional MF method and CS method, respectively. The horizontal axis is range

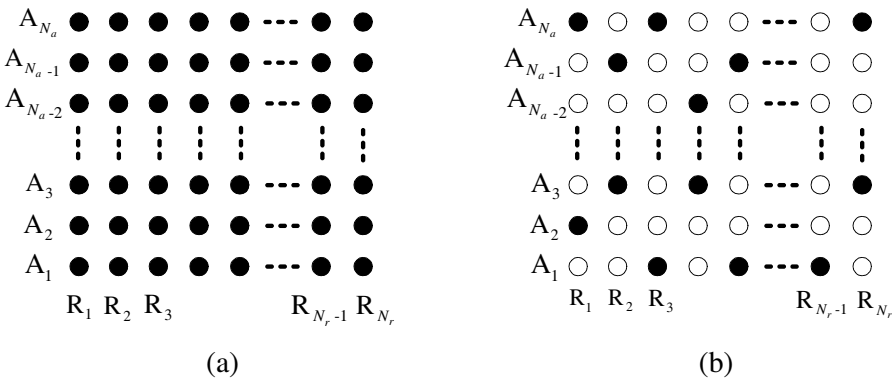

Figure 1. Samples acquisition for raw echo signal of SAR. (a) Tradition MF algorithm. (b) The CS method.

and the vertical axis is azimuth. The black points represent the echo samples acquisition in the range-azimuth plane. It shows that $N_a \times N_r$ samples follow Nyquist rate are a must in traditional SAR imaging method based on MF. However, only $M \ll N_a \times N_r$ random selected samples are required in CS method. In this paper, the black points selected for CS method are achieved as bellow. Firstly, a random permutation matrix $\mathbf{G} \in \mathbf{R}^{N_a \times N_r}$ of the integers $1 : N_a \times N_r$ is generated. Secondly, the indices of M largest values are found in matrix $\mathbf{G}$ elements. Lastly, M echo samples are selected from the SAR echo samples locations which are correspond to the indices obtained in the second step. Thereby, the presented method based on CS requires much fewer samples to construct the sparse target compared with traditional MF method.

Since the matrix $\boldsymbol{\Theta}$, vector $\mathbf{S}_p$ and $\boldsymbol{\alpha}$ are complex, in order to using CS reconstruction from the complex data, (15) should be rewritten as following.

$$\mathrm{Re}\left(\mathbf{S}_p\right) + j\mathrm{Im}\left(\mathbf{S}_p\right) = \left[\mathrm{Re}\left(\boldsymbol{\Theta}\right) + j\mathrm{Im}\left(\boldsymbol{\Theta}\right)\right]\left[\mathrm{Re}\left(\boldsymbol{\alpha}\right) + j\mathrm{Im}\left(\boldsymbol{\alpha}\right)\right] \tag{21}$$

The real and imaginary part of measured signal can be calculated respectively as

$$\begin{array}{l} \mathrm{Re}\left(\mathbf{S}_p\right) = \mathrm{Re}\left(\boldsymbol{\Theta}\right)\mathrm{Re}\left(\boldsymbol{\alpha}\right) - \mathrm{Im}\left(\boldsymbol{\Theta}\right)\mathrm{Im}\left(\boldsymbol{\alpha}\right) \\ \mathrm{Im}\left(\mathbf{S}_p\right) = \mathrm{Re}\left(\boldsymbol{\Theta}\right)\mathrm{Im}\left(\boldsymbol{\alpha}\right) + \mathrm{Im}\left(\boldsymbol{\Theta}\right)\mathrm{Re}\left(\boldsymbol{\alpha}\right) \end{array} \tag{22}$$

We define the signal $\hat{\mathbf{S}}$, $\hat{\boldsymbol{\alpha}}$ and $\hat{\boldsymbol{\Theta}}$ as

$$\hat{\mathbf{S}} = \begin{bmatrix} \mathrm{Re}\left(\mathbf{S}_p\right)^T \\ \mathrm{Im}\left(\mathbf{S}_p\right)^T \end{bmatrix}, \hat{\boldsymbol{\alpha}} = \begin{bmatrix} \mathrm{Re}\left(\boldsymbol{\alpha}\right)^T \\ \mathrm{Im}\left(\boldsymbol{\alpha}\right)^T \end{bmatrix}, \hat{\boldsymbol{\Theta}} = \begin{bmatrix} \mathrm{Re}\left(\boldsymbol{\Theta}\right) & -\mathrm{Im}\left(\boldsymbol{\Theta}\right) \\ \mathrm{Im}\left(\boldsymbol{\Theta}\right) & \mathrm{Re}\left(\boldsymbol{\Theta}\right) \end{bmatrix} \tag{23}$$

Then (19) further can be replaced as

$$\hat{\mathbf{S}} = \hat{\boldsymbol{\Theta}}\hat{\boldsymbol{\alpha}} + \mathbf{n} \tag{24}$$

4.3. Signal Reconstruction by CS

To recover the amplitude and phase of the sparse scattering centers in SAR echo signal, the sparsest solution can be solved by convex optimization based on l_1 norm.

$$\min \lambda \left\|\hat{\boldsymbol{\alpha}}\right\|_1 \text{ s.t } \left\|\hat{\mathbf{S}} - \boldsymbol{\Theta}\hat{\boldsymbol{\alpha}}\right\|_2 < \varepsilon \tag{25}$$

where the amount of noise ε can be estimated from measured data $\hat{\mathbf{S}}$ of echo signal. The main flow chart of imaging algorithm for SAR base on CS is shown in Figure 2.

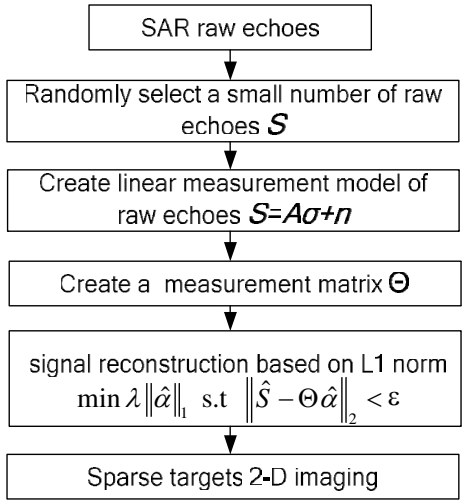

Figure 2. The flow chart of the presented CS method for SAR imaging.

5. SIMULTION AND DISCUSSIONS

In order to evaluate the performance of the presented method, in this section some numerical simulated experiments are presented at different SNR level and normalized measurements number M/N. The processing is also implemented for MF, and the results are compared between the two methods.

5.1. Imaging Evaluation

In this paper, the performance of the MF-based RD algorithm and the presented CS method for SAR imaging are evaluated in terms of three indicators: the peak sidelobe ratio (PSLR), the reconstruction relative error (RE) and a 3 dB beamwidth of point spread function.

PSLR is defined as the ratio which is peak intensity of the most prominent sidelobe to the peak intensity of the mainlobe.

$$\mathrm{PSLR} = 10\log_{10}\frac{\max\limits_{|x|<\rho_x,|y|<\rho_y}\left[\mathbf{H}^2(x,y)\right]}{\max\limits_{\rho_x<|x|<5\rho_x,\rho_y<|y|<5\rho_y}\left[\mathbf{H}^2(x,y)\right]} \tag{26}$$

where ρ_x and ρ_y denote the half width of mainlobe in range and in azimuth respectively, $\mathbf{H}(x,y)$ is the focused signal of point-scatter.

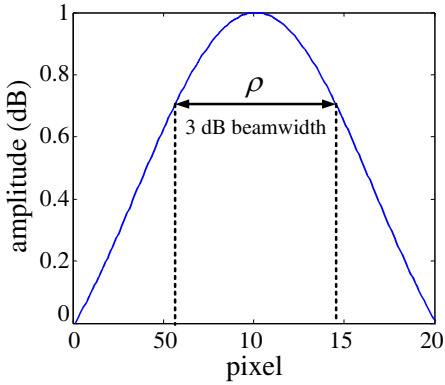

Figure 3. A 3 dB beamwidth of point spread function.

RE of reconstruction image is defined as follow.

$$\mathrm{RE} = \left\{ \frac{\sum_{x=1}^{M}\sum_{y=1}^{N}\left[\hat{\mathbf{I}}(x,y) - \mathbf{I}(x,y)\right]^2}{\sum_{x=1}^{M}\sum_{y=1}^{N}\left[\mathbf{I}(x,y)\right]^2} \right\}^{\frac{1}{2}} \tag{27}$$

where $\mathbf{I}(x,y)$ denotes the original image of scattering coefficients for illuminated scene, and $\hat{\mathbf{I}}(x,y)$ is the reconstructed one. Apparently, the lower the value of RE is, the better the reconstructed performance will be.

A 3 dB beamwidth of point spread function is an important indicator for the extracted target's scattering centers and it is shown in Figure 3. It is particularly suitable for the representation of spatial resolution in SAR imaging. Therefore, in order to achieve high resolution, the imaging method needs to obtain narrow 3 dB beamwidth.

5.2. Results and Discussion

Assume that SAR carrier frequency $f_c = 10\,\mathrm{GHz}$, the bandwidth of LEM signal $B_r = 150\,\mathrm{MHz}$, the number of slow-time samples and fast-time samples (both obey Nyquist rate) are $N_a = 64$ and $N_r = 64$ respectively, thus the total samples is $N = N_a \times N_r = 4096$. According to the resolution formula of MF method in (12), the range resolution is $\rho_r = 1\,\mathrm{m}$, and the azimuth resolution is $\rho_{at} = 1\,\mathrm{m}$. In this section, the simulations of two scenes are tested, one is a sample scene has nine

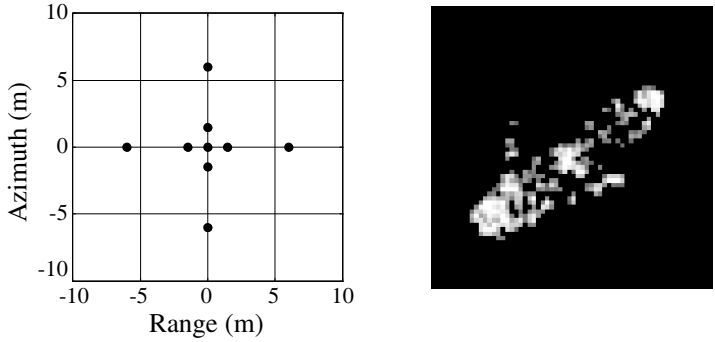

Figure 4. The original simulated scene. (a) Nine point targets. (b) A ship from ERS SAR image.

point targets, and another is a complex scene has a ship from ERS SAR image. The original scenes are shown in Figure 4.

Figure 5 shows the imaging results of nine point targets with different SNR level using both MF-based RD algorithm and the presented CS method respectively. The nine point scatterers have the same coefficient. The echo signals are added by Gaussian white noise with different signal noise ratio (SNR) level (noise free, SNR = 30 dB, 10 dB). The results of RD algorithm for the scene are shown in Figure 5(a). There is serious sidelobe interference in the imaging results using RD algorithm at all SNR level, and some details of positions or scattering coefficients of the targets are missing or fuzzy as the distance between adjacent targets are too close. Using the sparse information of the target space and solving the convex optimization problem, the results of the presented CS method using only 10% random samples at different SNR level are shown in Figure 5(b). At high SNR level, It is observed that the actual target positions and amplitudes are clearly reconstructed compared with the RD algorithm. In addition, the value of sidelobe in CS method is far less than that in RD method, and the resolution is improved even using a smaller sample size. At low SNR level, CS results have some false values in no target positions; But RD obtains almost the same results as high SNR because of MF processing can suppress noise.

Figure 6 shows the imaging results of the ship scene by MF-based RD algorithm and the presented CS method respectively. The original ship image from ERS SAR is shown in Figure 4(b). In order to facilitate analysis, the ocean scattering is ignored as it is very weak compared with ship scattering. The sparsity of original ship image

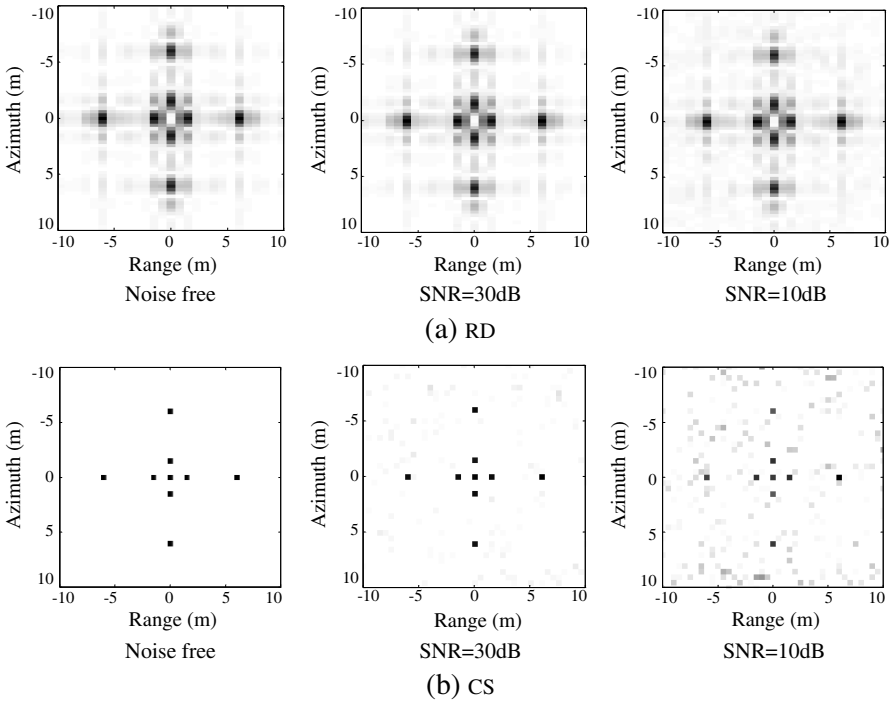

Figure 5. The imaging results of nine point targets with different SNR level. (a) The RD algorithm results using all samples. (b) The CS method results using only 10% echo samples.

$\zeta = K/N = 0.086$. The echo signals are also added by Gaussian white noise with different SNR level (noise free, SNR =20 dB, 10 dB). The imaging results of RD are shown in Figure 6(a). The imaging results of the presented CS method using 50% and 20% echo samples is shown in Figure 6(b) and Figure 6(c) respectively. The results show that the locations and scattering coefficients of ship scene are well extracted with low sidelobe by CS method at high SNR level, and some false targets appear at SNR = 10 dB. Compared with the traditional MF method, the presented CS method can significantly improve the imaging resolution of SAR when SNR is above 20 dB. Notably, the performance of CS relies on the number of measurements. The larger the number of echo samples are, the more scattering centers can be reconstructed.

To illustrate the resolution capability of CS method by a 3 dB beamwidth of point spread function, a simulation for single point target imaging is performed. Figure 7 shows the spectrum results of

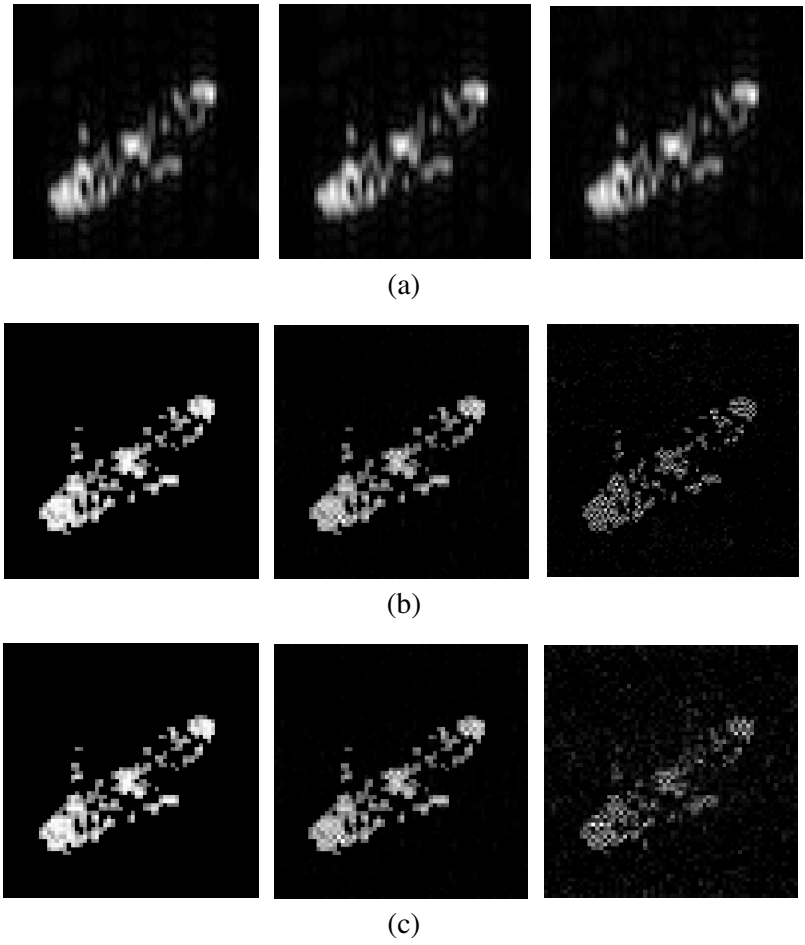

Figure 6. The imaging results of a ship scene with different SNR level. (a) RD algorithm results using all echo samples (left: noise free, middle: SNR = 20 dB, right: SNR = 10 dB). (b) and (c) are CS method results using only 50% and 20% echo samples (left: noise free, middle: SNR = 20 dB, right: SNR = 10 dB).

point spread function (PSF) at different SNR for both MF method and CS method respectively. According to the resolution formula of MF method, the spectrum is sinc function and the value of the maximum sidelobe is about −13.4 dB, and the 3 dB beamwidth of mainlobe is about 1 m. It is obvious that the spectrums of PSF of MF method are stable when SNR changes from noise free to SNR = 5 dB. When the data is noiseless, the value of the maximum sidelobe is

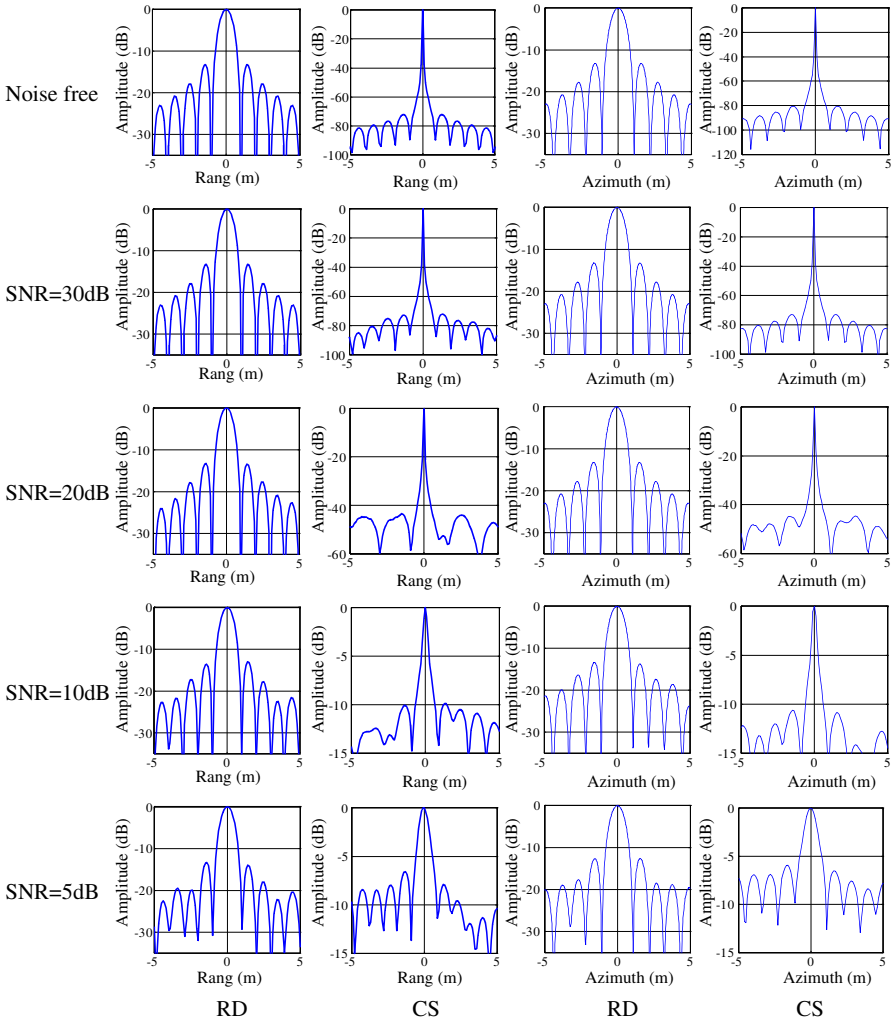

Figure 7. Spectrum of point spread function both in range and azimuth with different SNR level (Noise free, SNR = 30 dB, 20 dB, 10 dB, 5 dB).

about −81.3 dB in spectrums of PSF obtained by CS method, and the 3 dB beamwidth of mainlobe is apparently much smaller than that of MF method. However, the value of the maximum sidelobe is about −6.8 dB in spectrums of PSF obtained by CS method when SNR is 5 dB. Thereby, CS method is sensitive to noise, and the maximum sidelobe will increase as SNR decreases. If SNR is above 20 dB, the

3 dB beamwidth of PSF and the value of sidelobe of the presented CS method are both less than that of traditional MF method. Therefore, compared with the traditional MF method by 3 dB beamwidth, the presented method based CS significantly improves the resolution of SAR imaging at high SNR.

To analyze the influence of noise, imaging results of single point target for RD and CS methods with different signal noise ratio (SNR) are evaluated in terms of PSLR in Figure 8. At each SNR level, 100 independent trials are performed. The results of PSLR indicate that the presented CS imaging method is extremely better than MF method at high SNR (SNR $\geq$ 15 dB). It is notable that the number of measurements in CS method must be greater than $O\left(K\log(N/K)\right)$. A disadvantage of the CS imaging method is that it is sensitive to noise. Performance deteriorates with the decreases of SNR and the PSLR of CS method is lower than MF method when the SNR bellows 10 dB.

Figure 9 shows the RE of the constructed ship images by CS method versus the different normalized number of the measurements M/N and different SNR. The original image is shown in Figure 4(b). The RE of standard RD algorithm using all samples is 0.532. In Figure 9(a), the result demonstrates that the CS method outperforms the RD algorithm when the normalized number of the measurements is more than 0.16, but the performance of CS method begins to degrade markedly when the normalized number of the measurements is less than 0.16. Figure 9(b) plots the RE of Both RD with all samples and CS with only 20% random samples at different level of SNR at different SNR level. It is observed that the CS method has smaller RE than the RD method when the SNR is more than 15 dB. For the different SNR form 5 dB to 40 dB, the RE of imaging result of standard RD

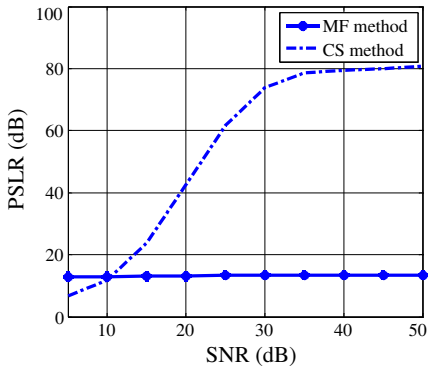

Figure 8. PSLR of the CS method and MF method at different SNR level.

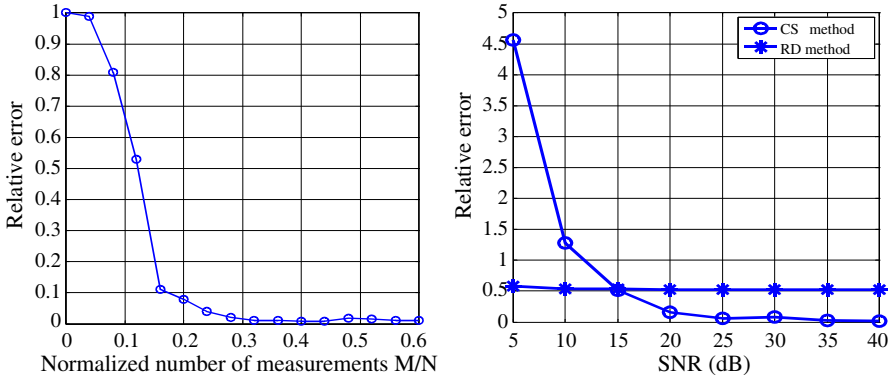

Figure 9. The relative error of ship scene reconstruction by CS method. (a) The RE versus the normalized number of measurements M/N for a $N = 4096$ original image with sparsity $K = 0.086$. (b) Comparison the RE of imaging results between the RD algorithm with all echo samples and the CS method with only 20% echo samples at different level of SNR.

method does not change too much because there is resolution limited for MF-based RD imaging. The presented CS method provides much lower RE when the SNR changes from 5 dB to 20 dB, and is stable for SNR $>$ 20 dB. This also indicates that the CS method outperforms the traditional MF-based RD method for the sparse target SAR imaging.

For the computation, MF method using RD is about $O[N\log_2(N)]$, and the presented CS method using basis pursuit is approximately $O\left(N^3\right)$. N is the measured sample. So the computation of CS method is always much higher than MF method. But in recent two years, some fast CS methods have been proposed, and the computation can be reduced to $O\left(NK^2\right)$, and K is the sparse targets. Compared with the traditional MF method, CS method increases the computational burden but obtains higher resolution with smaller measured samples.

6. CONCLUSION

This paper presents a sparse reconstruction method for SAR imaging based on CS theory, which aims at sparse targets reconstruction using less echo samples than Nyquist samples by solving convex linear problem. Compared with traditional MF-based RD imaging method, the presented method significantly suppresses the sidelobe and greatly

improves the imaging performance of SAR when the target space is sparse. Simulated results show a better performance of the presented method compared with traditional MF method. The sampling rate at SAR can be dramatically reduced. However, there are still some challenges need to be overcome in SAR imaging based on CS. The robustness of CS imaging needs to be improved with existence of serious noise.

ACKNOWLEDGMENT

This work was supported by the High-Tech Research and Development Program of China (No. 2007AA12Z118), the National Natural Science Foundation of China (No. 60772144).

REFERENCES

1. Soumekh, M., *Synthetic Aperture Radar Signal Processing with Matlab Algorithms*, Wiley, New York, NY, 1999.
2. Curlander, J. C. and R. N. McDonough, *Synthetic Aperture Radar: Systems and Signal Processing*, John Wiley and Sons, 1991.
3. Cumming, I. G. and F. H. Wong, *Digital Processing of Syethetic Aperture Radar Data: Algorithm and Implementatoin*, Artech House Publishers, 2005.
4. Chan, Y. K. and V. C. Koo, "An introduction to synthetic aperture radar (SAR)," *Progress In Electromagnetics Research B*, Vol. 2, 27–60, 2008.
5. Moreira, A., J. Mittermayer, and R. Scheiber, "Extended chirp scaling algorithm for air- and spaceborne SAR data processing in stripmap and ScanSAR imaging modes," *IEEE Transactions on Geoscience and Remote Sensing*, Vol. 34, No. 5, 1123–1136, Sep. 1996.
6. Fang, L., X. Wang, and Y. Wang, "A modified SPECAN algorithm for synthetic aperture radar imaging," *International Conference on Measuring Technology and Mechatronics Automation*, Changsha, China, Mar. 2010.
7. Donoho, D., "Compressed sensing," *IEEE Trans. Inf. Theory*, Vol. 52, No. 4, 1289–1306, Apr. 2006.
8. Baraniuk, R., "Compressive sensing," *IEEE Signal Processing*, Vol. 24, No. 4, 118–121, Jul. 2007.
9. Candes, E. J. and M. Wakin, "An introduction to compressive sampling," *IEEE Signal Processing Magazine*, 21–30, Mar. 2008.

10. Romberg, J., "Imaging via compressive sampling," *IEEE Signal Processing*, Vol. 25, No. 2, 14–20, Mar. 2008.
11. Bruckstein, A. M., D. L. Donoho, and M. Elad, "From sparse solutions of systems of equations to sparse mofeling of signals and images," *SIAM Review*, Vol. 51, No. 1, 34–81, Feb. 2009.
12. Gurbuz, A. C., J. H. McClellan, and W. R. Scott, Jr., "Compressive sens-ing for GPR imaging," *Proc. Asilomar Conf. Signals, Syst., Comput.*, 2223–2227, Nov. 2007.
13. Gurbuz, A. C., J. H. McClellan, and W. R. Scott, "A compressive sensing data acquisition and imaging method for stepped-frequency GPRs," *IEEE Transation on Signal Processing*, Vol. 57, No. 7, 2640–2650, Jul. 2009.
14. Huang, Q., L. Qu, B. Wu, and G. Fang, "UWB Throug-wall imaging based on compressive sensing," *IEEE Transactions on Geoscience and Remote Sensing*, Vol. 48, No. 3, 1408–1415, 2010.
15. Bhattacharya, S., T. Blumensath, B. Mulgrew, and M. Davies, "Fastencoding of synthetic aperture radar raw data using compressedsensing," *Proc. IEEE/SP Stat. Signal Process*, 448–452, Madison, WI, Aug. 2007.
16. Baraniuk, R. and P. Steeghs, "Compressive radar imaging," *Proc. IEEE Radar Conf.*, 128–133, Boston, MA, Apr. 2007.
17. Herman, M. A. and T. Strohmer, "High-resolution radar via compressed sensing," *IEEE Transactions on Signal Processing*, Vol. 57, No. 6, 2275–2284, Jun. 2009.
18. Zhang, L., M. Xing, C. Qiu, et al., "Achieving higher resolution ISAR imaging with limited pulses via compressed sampling," *IEEE Geoscience and Remote Sensing Letters*, Vol. 6, No. 3, 567–571, Jul. 2009.
19. Candes, E. J., J. Romberg, and T. Tao, "Robust uncertainty principles: Exact signal reconstruction from highly incomplete frequency information," *IEEE Trans. Inf. Theory*, Vol. 52, No. 2, 489–509, Feb. 2006.
20. Tropp, J. A., "Greed is good:algrorithmresults for sparse approximation," *IEEE Trans. Inf. Theory*, Vol. 50, No. 10, 2231–2242, Oct. 2004.
21. Needell, D. and R. Vershynin, "Uniform uncertainty principle and signal recovery via regularized orthogonal matching pursuit," *Found Comput Math*, Vol. 9, No. 3, 317–334, Jun. 2009.